Article:
Murray, J.J., Robert, C., Gleich, K. et al. (2020) Manufacturing of unidirectional stitched glass fabric reinforced polyamide 6 by thermoplastic resin transfer moulding. Materials & Design, 189. 108512. ISSN: 0264-1275

https://doi.org/10.1016/j.matdes.2020.108512

Materials and Design 189 (2020) 108512

Contents lists available at ScienceDirect

Materials and Design

journal homepage: www.elsevier.com/locate/matdes

Manufacturing of unidirectional stitched glass fabric reinforced polyamide 6 by thermoplastic resin transfer moulding

James J. Murray [a,*], Colin Robert [a], Klaus Gleich [b], Edward D. McCarthy [a], Conchúr M. Ó Brádaigh [a]

[a] School of Engineering, Institute for Materials and Processes, Sanderson Building, The University of Edinburgh, Robert Stevenson Road, EH9 3FB Scotland, UK
[b] Johns Manville Europe GmbH, Werner-Schuller-Str.1, 97877 Wertheim, Germany

HIGHLIGHTS

- In-situ polymerised polyamide composite was manufactured by resin transfer moulding.
- Bespoke thermoplastic resin transfer moulding equipment was designed and built.
- Polymer and composite properties (0° & 90°) were characterised mechanically.
- The longitudinal strength was superior to commercial organo-sheet.
- Reduced transverse strength due to the high packing density in bundles at stitch

GRAPHICAL ABSTRACT

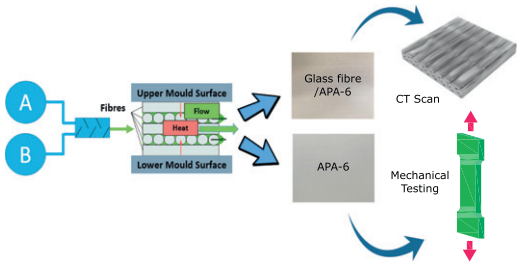

ARTICLE INFO

Article history:
Received 29 November 2019
Received in revised form 18 January 2020
Accepted 20 January 2020
Available online 21 January 2020

Keywords:
Thermoplastic resin
Mechanical properties
Resin transfer moulding
In-situ polymerisation

ABSTRACT

This study aims to address barriers which remain to adoption of reactive thermoplastic resin transfer moulding in terms of knowledge and equipment. Glass fibre reinforced polyamide 6 composites with ~52% fibre volume fraction and ~1% voids were produced within 5 min using thermoplastic resin transfer moulding by injection of low viscosity monomer precursors and in-situ polymerisation. Unidirectional laminates were produced using injection pressures of around 10% of those required to achieve the same fibre volume fraction and degree of wet-out using a typical thermoset RTM resin, negating the need for expensive equipment. The equipment and process employed are described in detail and the quality and properties of the polymer matrix and composite laminates were characterised extensively in terms of chemical, thermo-morphological and mechanical properties. The paper demonstrates the high quality parts that can be achieved by accurately controlling some of the most important parameters.

1. Introduction

Engineering and advanced engineering thermoplastics have unique properties that render them desirable as matrices for many composite applications where thermoset resins are unsuitable. Joining processes such as welding, manufacturing processes such as thermoforming and material recyclability are some of the many benefits to be realised from their use. Due to their high molecular weight, they are generally tougher than thermoset resins, and because they can be melted, their unique properties can be exploited and tailored for their application in composites. Their high molecular weights, however, also result in higher melt temperatures and higher melt viscosities, making them difficult to process. This makes liquid composite moulding (LCM) of thermoplastic melt with high fractions of continuous fibre reinforcement impractical, as extremely high pressures are required to infiltrate fibres and to achieve good fibre/matrix uniformity to ensure sufficient load transfer between fibre and matrix [1]. As a result, their use in composites has been limited to expensive intermediate materials such as commingled fabrics and pre-impregnated tapes which still require the

* Corresponding author.
E-mail address: j.j.murray@ed.ac.uk (J.J. Murray).

https://doi.org/10.1016/j.matdes.2020.108512

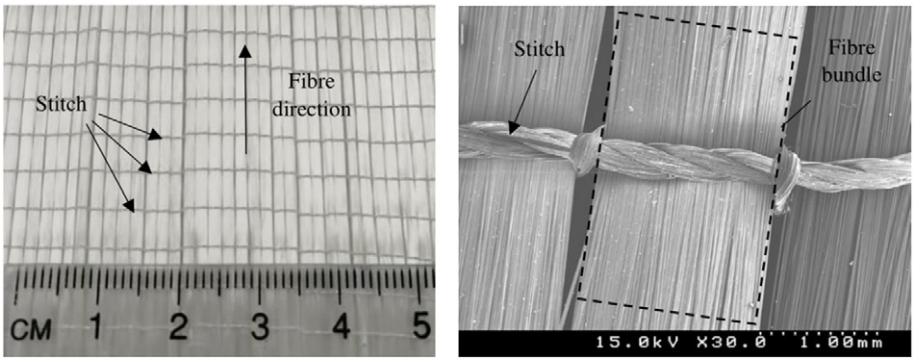

Fig. 1. Images of the stitched glass fibre NCF with polyester stitching.

application of additional pressure and temperature to manufacture parts [2,3].

The automotive industry in recent years has increasingly focused on weight (hence fuel consumption) reduction to reduce the environmental impact (CO_2 emissions) of vehicles, an approach which has been mandated by legislation [4,5]. With a recent global shift towards the use of electrical power sources, light-weighting is more important than ever to counter the weight of heavy batteries [6,7]. The use of high quality thermoplastic composites (TPCs) may be justified if the cycle times can be minimised to produce ~100,000 parts per year economically [8].

Resin transfer moulding (RTM) is a popular LCM process used to produce composite parts for high volume manufacturing where the cost of the equipment required can be justified [4]. The process involves injecting a resin under pressure in to a reinforcement fibre preform contained within a mould [9]. A press is often required to generate reaction forces to keep the mould closed during injection and prevent the cavity walls from deflecting. By mounting the mould halves to the platens, part removal speed can be reduced and cycle times increased as a result.

The development of reactive thermoplastic processing techniques in recent years has provided the means of enabling LCM of thermoplastics by injecting a low viscosity monomer precursor material and reactants as opposed to injecting the thermoplastic melt. After infiltration of fibres, the pre-mixed reactants polymerise in-situ, resulting in a thermoplastic composite part. There are a range of TP precursor systems on the market, which exploit this such as Elium®, an acrylic based system developed by Arkema which polymerises at room temperature [10]. Its drawbacks are the expense of the precursor and the large amount of heat generated by the reaction exotherm, particularly for thicker sections [11]. Work has been carried out in the past on composites with a polybutylene terephthalate matrix produced from cyclic oligomers (pCBT) that can be polymerised isothermally at ~180 °C, demonstrating reasonable mechanical properties. Due to its morphology after polymerisation at this temperature, the material is brittle, yields poor impact properties and often requires additives for toughening [12–14]. Wind turbine blades have successfully been manufactured from both Elium and pCBT using exothermic control additives for the former and specialised high temperature tooling for the latter [11,15]. Much work has been carried out on anionic ring opening polymerisation of lactams to produce polyamides [16–19]. Work on polyamide 12 (PA-12) composites produced from laurolactam has been carried out in the past but has largely been surpassed by research on polyamide 6 (PA-6) produced from caprolactam, mainly because PA-6 requires lower processing temperatures and its strength and modulus are superior [20–23]. The caprolactam monomer has a viscosity of <10 mPa.s at melt which is lower than some of the lowest viscosity thermoset resins used for RTM and can be polymerised in a fraction of the cure time [24].

Much of the literature published on anionically polymerised PA-6 (APA-6) composites derived from a renewed interest in the area after extensive research was carried out by Bersee [25–28]. This work was aimed at developing a vacuum infusion process to manufacture thermoplastic composite wind turbine blades but dealt with a broad range of more fundamental research on LCM of APA-6. These studies focused mainly on the effects of processing temperature and different types and quantities of activators/catalysts on the degree of polymerisation, crystallinity and mechanical properties. Work was carried out comparing the interfacial properties of composites using different fibre sizings; however, due to the large void content (up to 10% by volume) and the low repeatability of the vacuum assisted resin transfer moulding (VaRTM) process, uncertainty remains over some of the conclusions [29]. The resin flow rates can be difficult to control using vacuum as the driving force, due to the almost water-like viscosity of the precursors which are extremely sensitive to pressure changes. This means it is difficult to obtain adequate flow control even using fine control valves. If the vacuum pressure is too high, the flow rate is rapid and inter-bundle infiltration of fibres is poor. If the vacuum pressure is too low, polymerisation onset may occur before the liquid mixture reaches the outlet of the mould. Moreover, if the monomer is not heated to temperatures above 69 °C, the monomer in the feed lines will freeze, preventing further infusion. A more controlled process involves driving the precursors using an overpressure or set of pumps. This process is known as thermoplastic resin transfer moulding (TP-RTM). Most academic work published on TP-RTM to date, has used an overpressure of gas to drive the liquid precursors [23,30–33].

In more recent years, industrial partnerships between automotive companies, raw material suppliers, RTM injection system manufacturers and academic institutes have resulted in the successful serial manufacture of APA-6 composite parts using highly sophisticated manufacturing processes [34–40]. Such systems are generally expensive because they require the heating and pumping of two components above melt temperature at all times while almost completely

Table 1
Summary of raw material used to produce GF/APA-6 composites.

Material type	Product description	Brand name	Supplier
Monomer	ε-caprolactam	AP-NYLON® Caprolactam	Brüggemann
Catalyst	Sodium caprolactamate	BRUGGOLEN® C10	Brüggemann
Initiator	Hexamethylene-1,6-dicarbamoylcaprolactam	BRUGGOLEN® C20p	Brüggemann
Reinforcement	Polyester stitched UD glass fibre NCF	StarRov® 871	Johns Manville

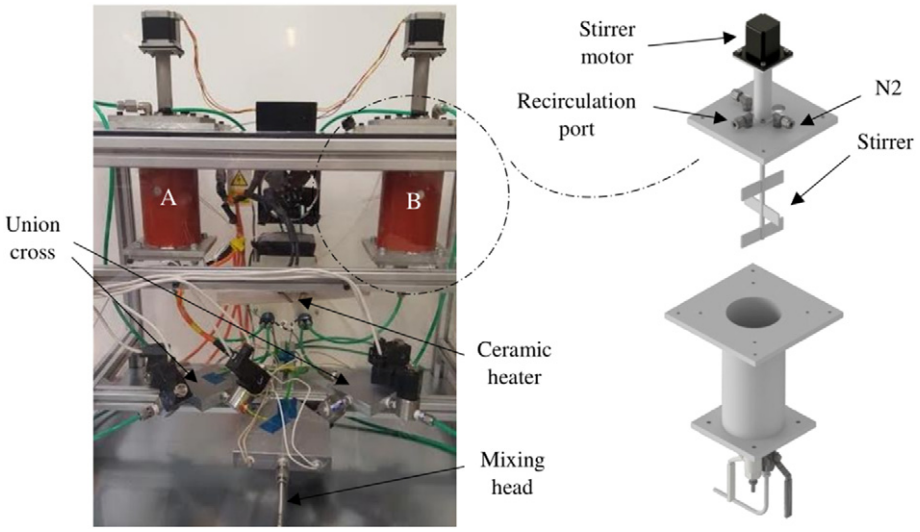

Fig. 2. TP-RTM machine components with a view of the tank parts with the top removed.

eliminating moisture in the system, making it more complex than standard RTM equipment. This complication, combined with the fact that there is a limited amount of experience in the general composites community in reactive processing, means that attempts at manufacturing APA-6 composites using quick, controlled processes have been avoided due to the risk involved. Despite the fact the technology exists to produce thermoplastic composites, and although engineers recognise their many advantages, there remain barriers to their deployment such as lack of design data and process experience in the composites community.

The main aims of this paper are to address knowledge gaps which remain in processing APA-6 composites by giving a detailed description of the equipment needed, the processing parameters required, and the material properties which result. Another aim is to demonstrate the part quality that can be achieved using the relatively inexpensive TP-RTM setup. The study focused on minimising voids, in order to achieve sufficient quality, and hence material properties. The pure polymer and unidirectional (UD) glass fibre composites produced using this method were characterised in-depth using various physical and mechanical approaches. These properties would be useful for finite element modelling and design of parts in the future as no UD properties for such GF/APA-6 composites have existed before this study. The results were benchmarked against properties of commercial UD organosheets produced from melt-processed GF/PA-6 for comparison.

2. Methodology

2.1. Materials and storage

The raw reactant materials used for polymerisation of the APA-6 composite matrix were the ε-caprolactam monomer (brand name AP-NYLON® Caprolactam), catalyst/caprolactam blend (brand name BRUGGOLEN® C10) and bi-functional initiator/caprolactam blend (brand name BRUGGOLEN® C20p). All the materials were supplied by Brüggemann GmbH & Co. KG (Heilbronn, Germany). Due to the sensitivity of the anionic polymerisation to moisture and the hydrophilic nature of the APA-6 precursor materials, extreme caution was taken to limit the exposure of the raw materials to moisture. The caprolactam was provided in flake form and once opened, each bag was sealed and stored in an airtight drum in a nitrogen atmosphere with desiccant. The BRUGGOLEN® C10 was also supplied in flake form, consisting of ~20: 80 wt% sodium-caprolactamate: caprolactam and the BRUGGOLEN® C20p was supplied in pellet form, consisting of ~80: 20 wt% hexamethylene-1,6-dicarbamoylcaprolactam: caprolactam. Both of these were stored in sealed bags contained in a glass desiccator at room temperature. Quantities of caprolactam, catalyst and initiator for between 4 and 8 injections were weighed out at a time to reduce the exposure time of the caprolactam to moisture. The measured quantities were stored in sealed glass powder jars with silica bags.

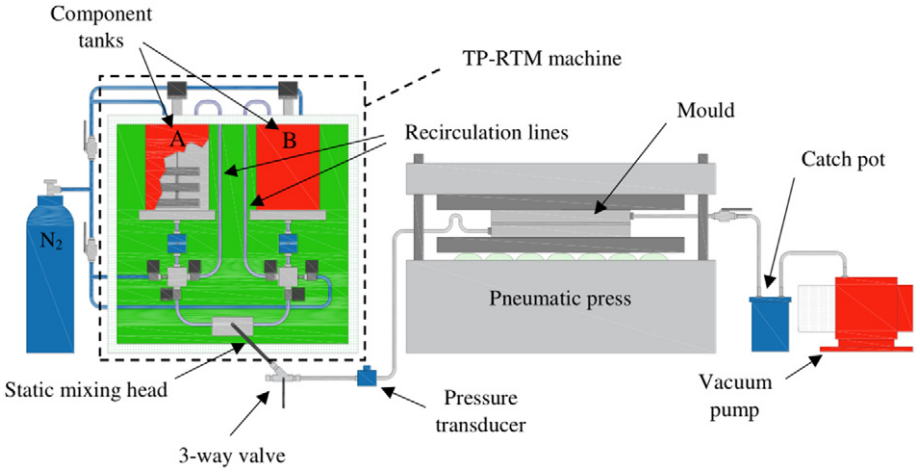

Fig. 3. TP-RTM setup during injection including the TP-RTM machine, pneumatic press, closed mould, vacuum pump and catch pot.

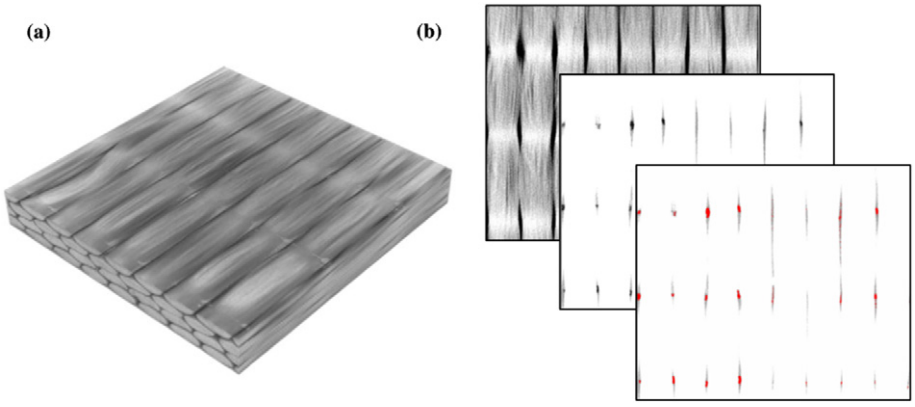

Fig. 4. (a) Stacked 3D view of one of the 15 mm × 15 mm CT samples and (b) visual representation of the image processing steps used to analyse the void content and distribution.

A 640 g/m^2 unidirectional stitched glass fibre non-crimp fabric (caprolactamNCF) was used for this study. The continuous glass fibre rovings (brand name StarRov® 871) used in the fabric were produced by Johns Manville (CO, USA) and were coated with a silane sizing that was compatible with in-situ polymerisation of APA-6. The rovings were made of 2200 single filaments, each with a diameter of ~17 μm. The fabric was stitched by DITF (Denkendorf, Germany) using polyester stitches perpendicular to the fibre direction in 5 mm increments as shown in Fig. 1. The fabric was stored in standard lab atmospheric conditions prior to the preparation stage, during which the cut fabric was dried in the closed mould for at least 90 min at 130 °C under vacuum. All the raw materials used and their suppliers are summarised in Table 1.

2.2. Resin transfer moulding equipment

A bespoke system to carry out resin transfer moulding of APA-6 composites was designed and built at The University of Edinburgh. The system consists of a TP-RTM machine for component mixing/injection, a pneumatic press, a closed aluminium mould and interconnecting parts to transfer and control the flow of the liquid precursors. The TP-RTM machine consists of two heated aluminium tanks for storage of the precursor materials with local temperature control, dynamic stirring and a nitrogen purge supply to create an inert atmosphere (see Fig. 2). A pair of stainless steel gear pumps is used to pump the liquid components in either recirculation mode, where the individual components circulate in a loop, or in injection mode where the two components are pumped through a static mixing head in a 1:1 ratio by volume. The flow route is controlled by electrically operated solenoid valves. A separate line transports nitrogen gas to the individual component lines to purge and flush the system before and after injection, respectively. Check valves are fitted to prevent a backflow of liquid into the nitrogen lines. All the machine components are contained within an insulated housing with convection heating supplied by a ceramic heater and fan such that the precursor materials are maintained above their melting point at all times. The global heating system and the localised tank heaters are controlled using PID controllers with control parameters set such that accurate and consistent temperatures are maintained.

A three-part mould is designed to manufacture laminates. The mould consists of two aluminium surfaces with interchangeable cavity plates of various thicknesses to accommodate for different specimen types in accordance with the appropriate test standard. Silicone rubber seals are used on either mould surface to prevent leaking of liquid precursor during injection and to retain a vacuum while drying the fibre reinforcements. When assembled, there is a single inlet port and a single outlet port at either end of the mould. A line injection gate encourages rectilinear filling of the cavity. The assembled mould is placed between two heated platens of a pneumatic press and a force of ~100 kN is applied to effectively seal the mould while handling injection at elevated pressures.

Aluminium tubing with an inner diameter of 4.6 mm is used to transport the mixed liquid precursors from the mixing/injection unit to the mould via a manually controlled 3-way ball valve and a pressure sensor (Composites Integration EL-35-0029). The voltage output signal from the sensor is measured using an Arduino Uno microcontroller and is recorded and monitored on a laptop. At the outlet of the mould, there is an aluminium tube connecting the mould to a ball valve. A hose coming from a vacuum pump is connected to the other end of the ball valve via a resin pot. The assembled setup is shown in Fig. 3. The TP-RTM machine was built for approximately £5000 excluding machining and labour costs. Extruded aluminium profiles were used for the frame, and the inner and outer walls were made from sheet aluminium with glass wool insulation. The choice of seal material that contacts the caprolactam is important as many standard elastomeric seal materials are not compatible with the precursor. Kalrez® perfluoroelastomer (FFKM) was used in these areas such as the plunger seal on the solenoid valves and o-ring in the check valves. Where a press is already available to host a mould, the system is relatively inexpensive to set up.

2.3. Manufacturing laminates

The mould surfaces, inlet and outlet, were cleaned using acetone, and two layers of mould release agent (Loctite Frekote 55NC) were applied prior to laying up the fabric in the mould cavity. All monomer residue from previous runs was dissolved from the aluminium tubes and ball valves using hot water at around 90 °C followed by air drying in an oven at 110 °C. For the 2 mm cavity, 4 plies of stitched unidirectional fabric were laid up with final dimension of 350 mm × 390 mm. Due to open stitches along the ply edges from cutting, additional material in the width-wise direction was allowed to account for lost fibre bundles during handling. After placement of the four plies, excess bundles were removed and the overhanging stitches were trimmed so that they would not act as a pathway for leaking between the seal and cavity plate. Due to the ease of fabric handling and the guidance of the cavity edges, good fibre alignment was achieved. The upper mould surface was placed on top of the other mould parts to close the cavity. The gap created by the seals was investigated along the perimeter to ensure

Table 2
Average values ± SD for thickness, density, fibre volume fraction and voids in the APA-6 polymer plate and GF/APA-6 laminates.

Plate	Thickness	Density	Fibre volume	Void volume
	t (mm)	ρ (g/cm^3)	V_f (%)	V_v (%)
APA-6	3.83 ± 0.07	1.147 ± 0.002	–	–
GF/APA-6 A	1.97 ± 0.07	1.883 ± 0.028	51.4 ± 2.0	0.8 ± 1
GF/APA-6 B	1.99 ± 0.06	1.882 ± 0.025	51.8 ± 1.9	1.1 ± 0.4

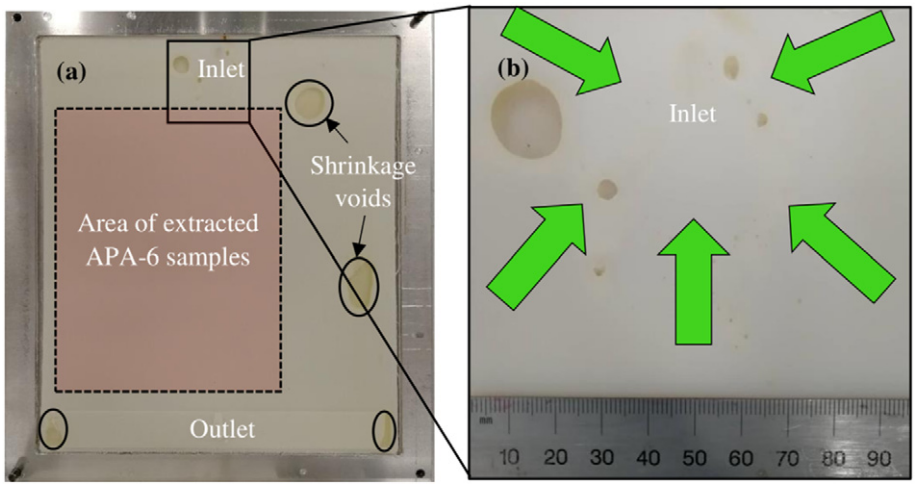

Fig. 5. (a) Image of an APA-6 plate in the mould cavity and (b) a close-up view of voids due to shrinkage around the inlet of the mould.

that it was consistent and that there were no fibres or stitches to be seen.

The assembled mould was placed between the platens of the pneumatic press, and the aluminium tube for the outlet was secured to the mould with the valve and vacuum accessories connected. The aluminium tube, sensor, and 3-way valve were connected at the inlet side of the mould. The valve was initially positioned to shut off flow such that the cavity could be used as a vacuum chamber during drying. The vacuum pump with a pump rate of 330 dm^3/min was turned on, pressure was applied to the mould, and the platens were heated to 130 °C for at least 90 min for sufficient drying of the fabric to occur. The vacuum pressure was monitored with the sensor at the inlet and from the pressure gauge on the catch pot at the outlet. Typical gauge pressure readings of around - 990 and − 980 mbar respectively indicated that a sufficient vacuum was achieved.

The local tank temperatures were set to 100 °C and the global temperature of the enclosed parts were set to 90 °C. The system was flushed with caprolactam before each run to remove any moisture that may have been present on the inner walls of the machine components. Precursor materials consisting of 98.2 mol% caprolactam, 0.6 mol% bifunctional activator and 1.2 mol% catalyst were poured in to the component tanks. The stirrers were turned on and the tanks were purged with nitrogen gas to create an inert atmosphere while heating. The vacuum was then reduced such that the absolute pressure in the mould was just higher than the vapour pressure (53 mbar) of the precursor components at the exothermic temperature peak (~170 °C), but sufficiently low to prevent large amounts of air entering the mould and hence oxidising the sizing [41]. Nitrogen was purged through the component lines and the mixing head and exited through the bleed port of the 3-way valve in order to purge the liquid precursor carrying components which were not under vacuum. The components that were now melted in the tanks were then recirculated, followed by injection at a flow rate of 820 dm^3/min. In order to bridge the gap between the liquid precursor flow front and the vacuum, the air/nitrogen gas mixture in front was bled through the bleed port of the 3-way valve until a consistent flow was observed, at which point the valve was adjusted such that the flow was directed into the mould. When the mixed liquid precursors reached the mould outlet, the ball valve at the outlet was manually adjusted to partially restrict the flow such that the pressure was increased to ~4 bars while still flowing. After holding for several seconds, the valve at the outlet was shut, then the inlet valve was closed, and finally the pumps were turned off.

15 min after injection, the heating to the platens was turned off but the pressure was maintained such that both sides would cool naturally at the same initial rate of approximately 2.7 °C/min. The laminates were demoulded at room temperature.

2.4. Sample preparation

All samples were prepared in a similar manner, apart from pure polymer tensile and dynamic mechanical analysis (DMA) samples. All polymer samples were extracted from a single panel and all composite samples came from one of two laminates with very similar thickness, density and fibre volume fraction (methodology for measurement is discussed further in Section 2.5). The samples were cut using a diamond blade cutting saw with coolant at a feed rate of ~300 mm/min. Due to their complex geometry, the polymer tensile samples were cut using a CNC machine with coolant using a high speed steel cutter at 5000 RPM and a feed rate of 230 mm/min. Samples for differential scanning calorimetry (DSC) were cut using a Stanley knife blade. All samples were then dried under vacuum for 24 h at 50 °C and stored in polybags with desiccant until testing.

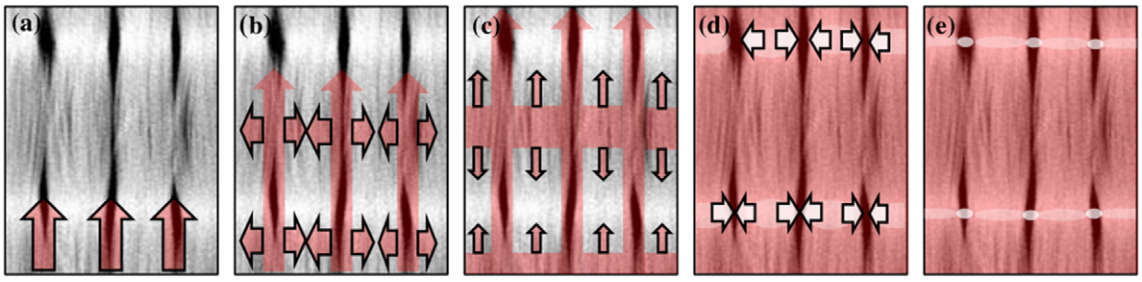

Fig. 6. Suspected formation of voids during injection where red indicates the liquid precursors and white indicates gas. The steps include (a) Macro-flow making its way through a ply, (b) radial flow into fibre bundles, (c) capillary driven intra-bundle flow towards the stitched areas, (d) expulsion of air in to inter-bundle regions, (e) resulting macro and micro voids after application of ~4 bars of pressure.

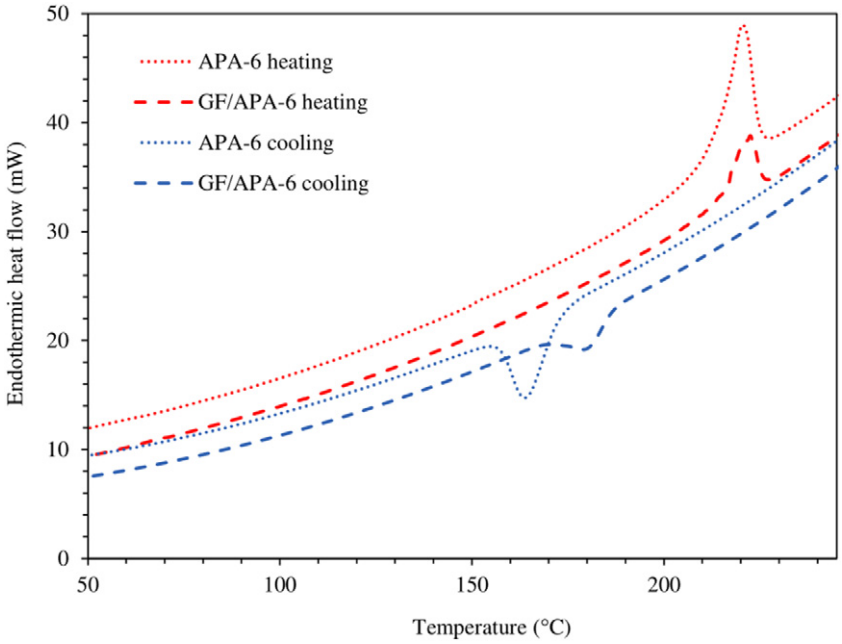

Fig. 7. Typical heat flow-temperature curves for the APA-6 polymer and glass fibre reinforced APA-6.

2.5. Thickness and density

The thickness variation of the pure polymer and composite was measured using a Kroeplin Digital C450 electronic measuring gauge, which is accurate to the nearest 0.02 mm. The measurements were taken at 25 locations evenly distributed in a 5 × 5 pattern across each plate/laminate.

The densities of both the pure polymer and composite were determined for 15 mm × 15 mm samples taken from 9 locations evenly distributed across all plates/laminates. The mass of each sample was measured in both air and water using an OHAUS AX324 analytical balance and a density determination kit. An overhanging bracket was fixed to the scale, and a glass beaker with distilled water was placed on a platform below it. The temperature of the distilled water was recorded using a thermometer such that its density could be accurately determined. A sample holder was hung from the overhanging bracket and submerged in the water. After zeroing the setup, the sample was added to the holder and the apparent mass in water was recorded. The density was determined using Archimedes' principle based on the mass difference between the two measurements in accordance with *ISO 1183-1:2019 Method A.*

2.6. Fibre volume fraction and void determination by burn-off

To determine the fibre volume fraction (V_f) of composite samples, the 9 samples from the density measurements were used for burn off in accordance with *ISO 7822:1999-Method A*. The samples were placed in ceramic crucibles, and the total weight of each was measured. Lids were put on the crucibles, and they were placed in the furnace. The samples were heated from room temperature to 560 °C over the course of an hour and were held at this temperature for 5 h to allow burn off of the matrix. After completion of the heating cycle and cooling back to room temperature, the crucibles containing the fibres only were weighed, and V_f was determined using known fibre and matrix density values. With knowledge of these properties as well as composite density and fibre volume fraction, the void content was calculated.

2.7. Void content validation by computerised tomography scans

In addition to the measurement of the void content by volume, the distribution of voids and their significance was required to later explain mechanical test results. To do so, one-off computerised tomography (CT) scans were carried out on 9 composite samples (dimensions: 15 mm × 15 mm) taken from a different laminate manufactured in a similar manner. 3D representations of the samples were produced by stacking the individual CT images (~80 per sample) using *ImageJ* software. The brightness of the stack was increased to filter out the visible range dominated by the fibres, such that greater contrast could be presented in the resin-rich inter-bundle trenches where the macro voids were located. The macro void content by volume was determined using thresholding segmentation on *ImageJ*. The image processing steps are presented in Fig. 4. The 9 samples were then burnt off following the method described in Section 2.6 such that the void content methods could be compared.

2.8. Degree of conversion, crystallinity and melt

To determine the degree of monomer conversion to polymer during polymerisation, a reflux extraction method was used to dissolve and extract the monomer. Approximately 100 g of composite from each laminate was milled to small pieces using a CNC milling machine. The

Table 3
DSC results for the pure APA-6 and GF/APA-6 composite samples.

Plate	Melt peak temperature	Enthalpy of fusion	Avg. resin weight fraction	Degree of crystallinity as processed	Degree of crystallinity after 10 °C/min. Cooling
	T_m (°C)	ΔH (J/g)	W_p (%)	X_{c1} (%)	X_{c2} (%)
APA-6	219.4 ± 1.0	75.3 ± 5.5	100*	42.2 ± 3.1	20.5 ± 1.0
GF/APA-6 A	221.7 ± 0.9	23.2 ± 0.9	29.0	44.8 ± 1.7	20.2 ± 1.1
GF/APA-6 B	221.4 ± 0.9	23.7 ± 0.9	28.4	45.7 ± 1.7	19.9 ± 1.1

Table 4
Mechanical test results of APA-6 polymer specimens.

Test type	Maximum Strength (MPa)	Yield Strength (MPa)	Modulus (GPa)	Strain at maximum strength (%)	Strain at break (%)
Tension	83.2 ± 1.3	69.2 ± 2.4	2.8 ± 0.2	22.0 ± 0.5	29.5 ± 2.6
Flexure	102.7 ± 1.6	–	3.2 ± 0.2	6.2 ± 0.2	>> 9

milling of the sample maximised the surface area-to-volume ratio, improving the ease of extraction. The milled samples were then dried under vacuum for 24 h, weighed using an analytical balance and then placed in a round bottomed flask containing distilled water with a condenser fixed to it. The samples were refluxed in boiling water at 110 °C for 24 h to dissolve the monomer and low quality oligomer [42]. The samples were then dried again for another 24 h and their weight measured to determine the weight loss that was primarily attributed to the lost monomer. The samples were then heated in a furnace at 560 °C to burn off the polymer so that the mass of the fibres could be determined, thus allowing for approximation of the converted polymer content (DC) using Eq. (1) where m_m is the mass lost during extraction, m_t is the mass before extraction and m_f is the mass of the fibres.

$$DC \approx 100 - [m_m/(m_t - m_f)] \quad (1)$$

Differential scanning calorimetry (DSC) was used to determine the melt temperature and degree of crystallinity X_c for both the APA-6 pure polymer and GF/APA-6 composite cases. In order to determine X_c, it was necessary to measure the endothermic enthalpy change upon melting, ΔH_m. The samples underwent an isotherm for 2 min at 25 °C prior to heating at 10 °C/min. The samples were weighed and their mass m_s recorded prior to burn-off to determine the fibre mass m_f. The degree of crystallinity was calculated as follows where ΔH_c is the enthalpy of melt for 100% crystalline PA-6 with a value of 190 J/g from literature [43]:

$$X_c = (\Delta H_m/\Delta H_c) \times [(m_s/(m_s - m_f)] \times (1/DC) \quad (2)$$

2.9. Mechanical testing of polymer

2.9.1. Polymer tensile testing

Tensile tests of the pure polymer was carried out in accordance with *BS EN ISO 527-1:2012* using type 1B dumb-bell-shaped specimens. The tests were carried out on an Instron 3369 test machine using a 10 kN load cell and mechanical wedge grips. Specimens were coated with a speckled pattern using a fine black marker to create contrast differences to the specimens such that strain measurements could be measured using an IMETRUM video gauge. A crosshead speed of 1 mm/min was used during the test, and the modulus was calculated using video gauge strain data. Due to extensive deformation in the plastic region, nominal strain values at break had to be determined from crosshead extension measurements with respect to gauge length. These values were correlated with those measured using the video gauge in the linear region such that a compliance factor could be used to more accurately approximate strain at failure.

2.9.2. Polymer flexural testing

Flexural tests of the pure polymer were carried out in accordance with *BS EN ISO 178:2010 + A1:2013* in three-point loading using the specified loading support/nose radii, specimen dimensions (80 mm × 10 mm × 4 mm) and span of 64 mm. An Instron 3369 screw-driven machine was used with a 50 kN load cell. The midspan deflection of specimens was tracked using the video extensometer, i.e., the values used to calculate flexural strain and modulus by tracking a speckled pattern on the edge of samples. A crosshead speed of 2 mm/min was used, and samples were tested to approximately 9% flexural strain, at

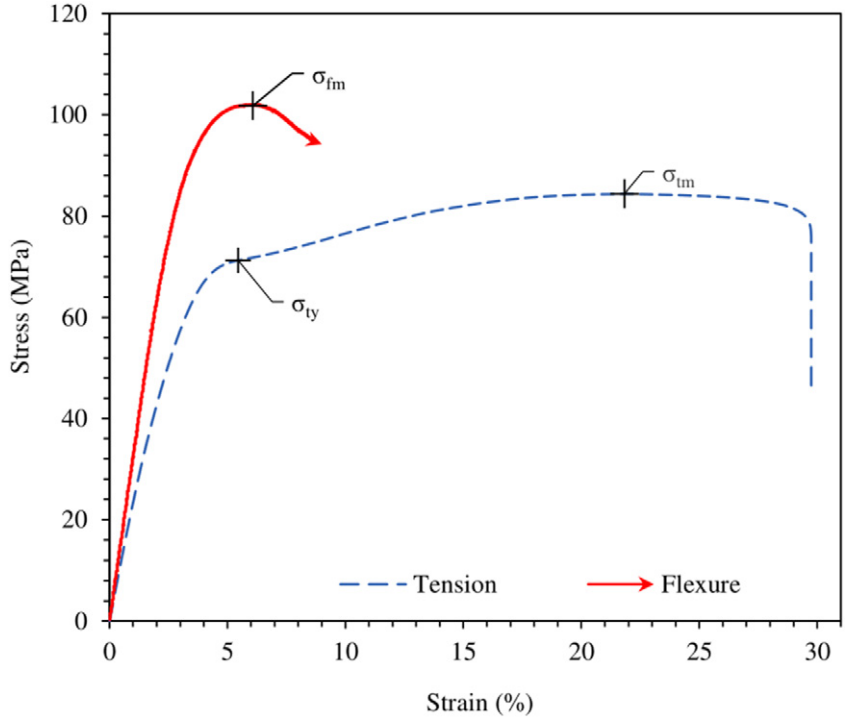

Fig. 8. Mechanical test results of APA-6 polymer where σ_{ty} represents the yield strength in tension and σ_{tm} and σ_{fm} represent the maximum strength in tension and flexure respectively.

Table 5
Transverse test results for the GF/APA-6 composite.

Test type	Maximum Strength (MPa)	Modulus (GPa)	Strain at break (%)
Tension (90°)	37.8 ± 2.4	10.6 ± 0.6	0.4 ± 0.0
Compression (90°)	134.7 ± 5.3	12.3 ± 0.9	2.7 ± 1.0
Flexural (90°)	82.8 ± 9.8	10.3 ± 0.5	1.1 ± 0.1

which point the samples came in contact with the three-point bending fixture, rendering test results no longer valid beyond this point.

2.10. Mechanical testing of composite

2.10.1. Composite tensile testing

Tensile tests for the composite case were carried out in the transverse and longitudinal directions in accordance with *BS EN ISO 527-5:2012*. Type B specimens (250 mm × 25 mm × 2 mm) were used for transverse testing using an Instron 3369 screw-driven machine with a 10 kN load cell and a crosshead speed of 1 mm/min in order to keep the thickness in line with other test types, the dimensions of the longitudinal specimens used were 250 mm × 15 mm × 2 mm. The gripping ends of the specimens were sand blasted and cleaned with acetone prior to applying glass fibre end tabs which were bonded using a cyanoacrylate adhesive (Loctite 406) and polyolefin primer (Loctite 770). The samples were tested on an MTS C45.305 machine using a 300 kN load cell and a crosshead speed of 2 mm/min. A clamping pressure of ~70 bars was used to hydraulically grip the specimens. The strain for both the transverse and longitudinal samples was measured using the video extensometer and a speckled pattern. The Poisson's ratio for the longitudinal specimens was determined using strain measurements in the x and y directions during testing.

2.10.2. Composite compression testing

Compression tests were carried out in the transverse and longitudinal directions in accordance with *ASTM D6641/D6641M* using a combined loading compression (CLC) fixture using *Procedure A*. The fixture used in this test subjects the specimens to combined end- and shear-loading [44]. The specimens used were approximately 140 mm × 13 mm × 2 mm for both the transverse and longitudinal cases. They were placed in the fixture and tightened by applying a torque of 4 Nm to each of the 8 clamping screws. The fixture was placed between two compression platens fixed to the grips of an MTS C45.305 machine using a 300 kN load cell. A crosshead speed of 1.3 mm/min was used and strain was measured on one side by tracking a speckled pattern previously applied to the surface along the gauge length of specimens.

2.10.3. Composite flexural testing

Flexural testing of the composite were carried out in the transverse and longitudinal directions in accordance with *BS EN ISO 14125:1998 + A1:2011* in four-point bending using the preferred loading support/nose radii, specimen dimensions (60 mm × 15 mm × 2 mm) and span of 45 mm. An Instron 3369 screw-driven machine was used with a 50 kN load cell. The midspan deflection of specimens was tracked using the video extensometer by tracking a speckled pattern on the edge of samples. A crosshead speed of 1 mm/min was used and samples were tested to failure.

2.11. Scanning electron microscopy

Scanning electron microscopy (SEM) was used to study the fracture surface topography of failed flexural specimens as they had been subject to both compressive and tensile fracture. In order to separate the two halves of the specimens, the tests carried out in Section 2.10.3 were continued by further loading/deflecting the samples until significant tensile fracture occurred on the bottom surface. At this point, the deflections became so large that loading and support fixtures risked coming in contact with one another so the final separation was carried out by hand. The samples were firstly sputtered with a 200 Å thick gold coating to improve surface conductivity. A JEOL JSM-6010PLUS/LV SEM was used to observe samples at magnifications between 300 and 1200 at an accelerating voltage of 20 kV. A Carl Zeiss SIGMA HD VP Field Emission SEM was used to observe finer morphological features (<100 nm) at higher magnifications between 4800 and 60,000 with an accelerating voltage of 2 kV.

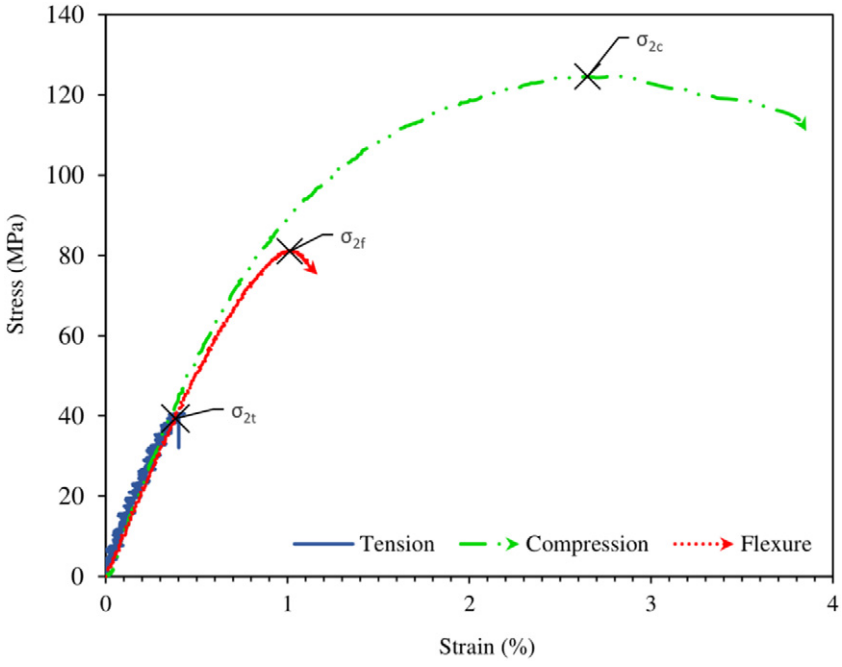

Fig. 9. Transverse mechanical test results of GF/APA-6 composite where σ_{2t}, σ_{2c} and σ_{2f} represent the maximum transverse strength in tension, compression and flexure respectively.

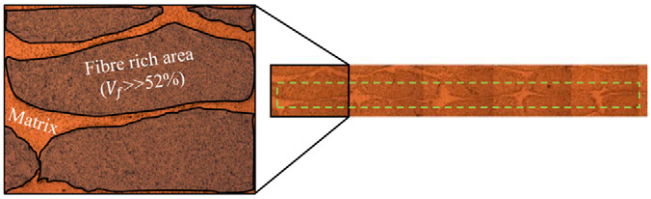

Fig. 10. Micro-section of GF/APA-6 composite to demonstrate the fibre rich intra-bundle and resin rich inter-bundle areas. The section was taken at a plane perpendicular to the fibre direction.

Table 6
Longitudinal test results for the GF/APA-6 composite.

Test type	Maximum Strength (MPa)	Modulus (GPa)	Strain at break (%)
Tension (0°)	1108.9 ± 66.3	40.8 ± 1.3	2.9 ± 0.1
Compression (0°)	691.1 ± 70.3	42.2 ± 1.7	1.7 ± 0.2
Flexural (0°)	1148.8 ± 54.5	37.8 ± 1.8	3.2 ± 0.1

3. Results and discussion

3.1. Quality assurance and observations

The quality assurance results in terms of thickness, density, fibre volume fraction and void content were determined based on analysis carried out on samples from evenly distributed locations on plates and are summarised in Table 2. The results demonstrate the degree of accuracy and consistency across the geometry of each plate and between different composite laminates used for testing throughout the rest of this study. Whilst the method used for void content determination is satisfactory for gaining approximate values, it is not very accurate [43].

3.1.1. Polymer plate quality

Due to shrinkage in the 4 mm × 350 mm × 390 mm cavity, a final average thickness of 3.83 mm was achieved for the pure APA-6 plate indicating ~4.3% reduction in thickness. A reduction in width of ~3.4% was observed along the central plane of the laminate perpendicular to the bulk flow direction from 350 mm to 338 mm. As the outlet is on the upper surface of the mould, it acts as a riser, supplying a supplementary feedstock of caprolactam to replace that from volume reduction during polymerisation. It is believed that the inlet acts in a similar manner initially because of the U-bend purposely introduced in the tube. However, because the inlet tube wasn't heated or insulated, the caprolactam feed at the inlet froze before significant conversions in the mould could be reached. Not only did this prevent further supply feed to the inlet but it also caused liquid precursor inside the mould to be dragged back towards the inlet tube. A large number of shrinkage induced voids were present at the inlet as a result (see Fig. 5(b)). Due to shrinkage in areas where the supplementary feedstock supply was cut off due to surrounding areas that were polymerised, some large voids were present in other locations in the panels as can be seen in Fig. 5(a). These voids were very discrete, and though large in size, there weren't many present. The surface was generally very smooth with no defects so specimens were extracted from the area shown in red in Fig. 5(a).

3.1.2. Composite laminate quality

Due to the use of a smaller cavity size of 2 mm and a 51–52% fibre volume fraction, about one quarter the volume of polymer was used in the composite laminates compared to the pure polymer plates. To a large degree, the presence of the glass fibres hindered geometric changes and subsequent defects which would otherwise occur as a result of resin shrinkage. The difference in cavity thickness and final part thickness was ~0.5–1.5% and no notable voids due to shrinkage, boiling or dissolved gas were observed. The voids present in the laminate were almost purely attributed to gas entrapped within the fabric. This will be discussed in more detail in Section 3.1.3. The low standard deviation for the four quality metrics indicates consistent properties throughout the geometry of the laminates, giving further validation to mechanical test results which will be discussed later. The similarity in values between laminates GF/APA-6 A and GF/APA-6 B demonstrate the consistency between the two, allowing greater justification to draw links between test samples extracted from different laminates.

3.1.3. Void content validation by CT

The inter-bundle void content of one laminate was measured using CT and compared to burn-off methods carried out on the same samples. Due to the low resolution of the scans, intra-bundle voids could not be determined whereas the burn-off method accounts for all voids. CT samples gave void values that were 50 ± 0.27% of that determined by burn-off, indicating that the macro-voids and micro-voids make up

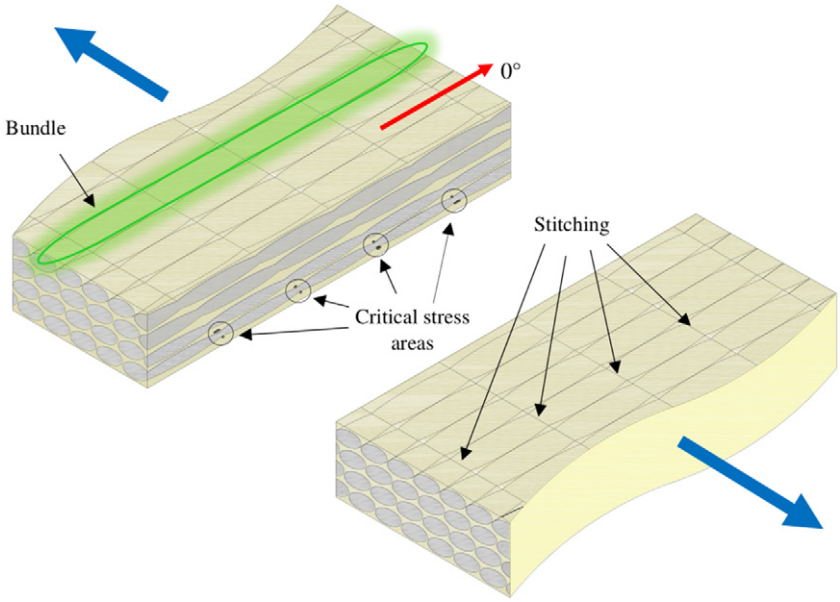

Fig. 11. Sketch of specimen loaded in tension in the transverse direction, demonstrating critical stress areas at stitch locations where the fibres are densely packed.

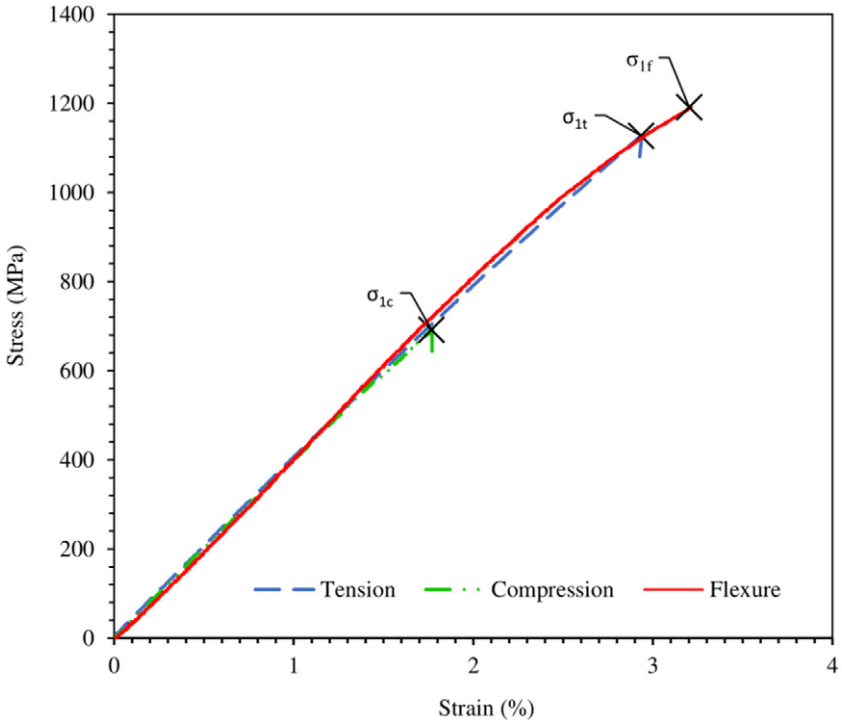

Fig. 12. Longitudinal mechanical test results of GF/APA-6 composite where σ_{1t}, σ_{1c} and σ_{1f} represent the maximum longitudinal strength in tension, compression and flexure respectively.

approximately the same volume. As suspected from visual observation of Fig. 4, macro-voids were present in areas along the stitch but otherwise, there were little voids observed. Their presence can be explained by entrapped air in the fabric during processing. A small amount of air enters the mould when the vacuum is reduced just prior to injection to prevent the liquid precursors boiling. The volume of air in the mould during injection can be determined from Boyle's law (Eq. (3)), where V_m is the volume of the mould and inlet tube, and P_{atm} and P_{vac} are the atmospheric pressure and vacuum pressure, respectively.

$$V_a = P_{vac}/P_{atm} \times V_m \tag{3}$$

For a 5.3 kPa pressure under vacuum, this results in around 5.2% air inside the cavity and tubing which is available for entrapment. In the case where no fibres are present, such as that for the pure APA-6 plate, this gas would be evacuated during injection as it is pushed out in front of the liquid precursors. The flow is much more complex for the composite case as air already exists within fibre bundles and becomes entrapped. As the macro-flow between the bundles moves forward, it is speculated that the liquid precursors also infiltrate radially into the fibre bundles but at a slower rate. This infiltration would occur primarily in the areas of least resistance where the fibres are less densely packed, i.e., at inter-stitch areas away from the fibre-stitch interfaces, where permeability is lower. This would be followed by capillary action, which would drive the intra-bundle flow from the inter-stitch regions towards the stitched regions. Because the fibre bundles are tightly packed at the stitch, it is likely that the intra-bundle flow would get choked. The capillary pressure would expel some of this air into the inter-bundle regions as the pressure in these regions would be less than that required to penetrate the stitched areas. The result is areas of both macro and micro voids in laminates at 5 mm increments. When the cavity pressure is then increased to 4 bars, the volume of these voids decreases. The steps of void formation are summarised in Fig. 6.

A possible solution to reduce this effect would be to use a greater vacuum to reduce the amount of air available for this phenomenon to

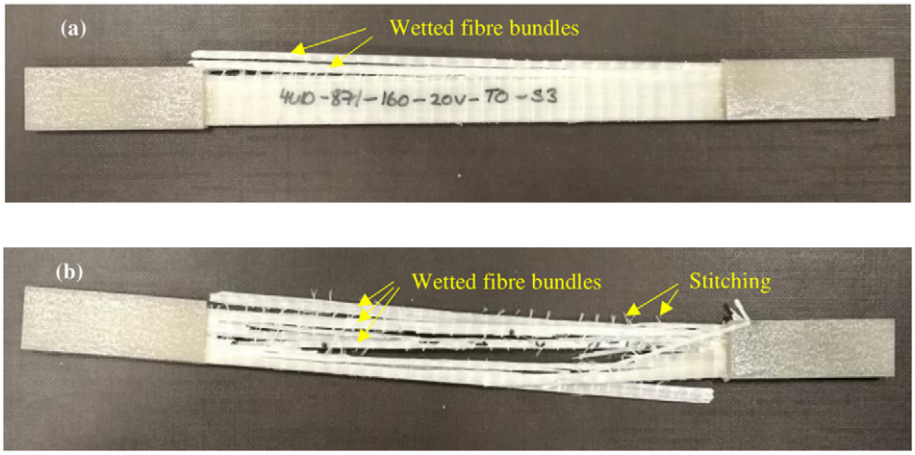

Fig. 13. Images of failed longitudinal tensile specimens after (a) initial failure, and (b) complete failure. In both cases, failure propagated along the matrix between wetted fibre bundles.

Table 7
Mechanical test results compared to commercially available PA-6 organo-sheet where the 0° values have been normalised to 50% fibre volume fraction. The organo-sheet values are from various sources: * SGL GF-PA6 UD-tape [50], **Evonik VESTAPE [53], ***TenCate TC910 [54] normalised to a fibre volume fraction of around 50%.

Mode	Strength (MPa)			Modulus (GPa)		
	Organo-sheet	Normalised GF/APA-6	Increase	Organo-sheet	Normalised GF/APA-6	Increase
Tension (0°)	1050*	1070.4	+1.9%	46*	39.4	−14.3%
Tension (90°)	40**	37.8	−5.5%	7.1**	10.6	+49.3%
Compression (0°)	431***	667.1	+54.8%	–	40.7	–
Compression (90°)	–	134.7	–	–	12.3	–
Flexure (0°)	1085*	1117.5	+3%	42*	36.8	−12.4%
Flexure (90°)	65*	82.8	+27.4%	10*	10.3	+3%

occur. While this can easily be accomplished, it is limited by the boiling of caprolactam at lower pressures, and reaction temperature is also a key factor. For example, at 163 °C, the vapour-pressure of caprolactam is ~4 kPa but at 147 °C, this is ~2 kPa indicating that a lower polymerisation temperature would allow a greater vacuum to be used and hence, greater void reduction would be achieved [41]. Though CT scanning is often considered the pinnacle of void content determination methods, a sufficiently high resolution is required to observe the

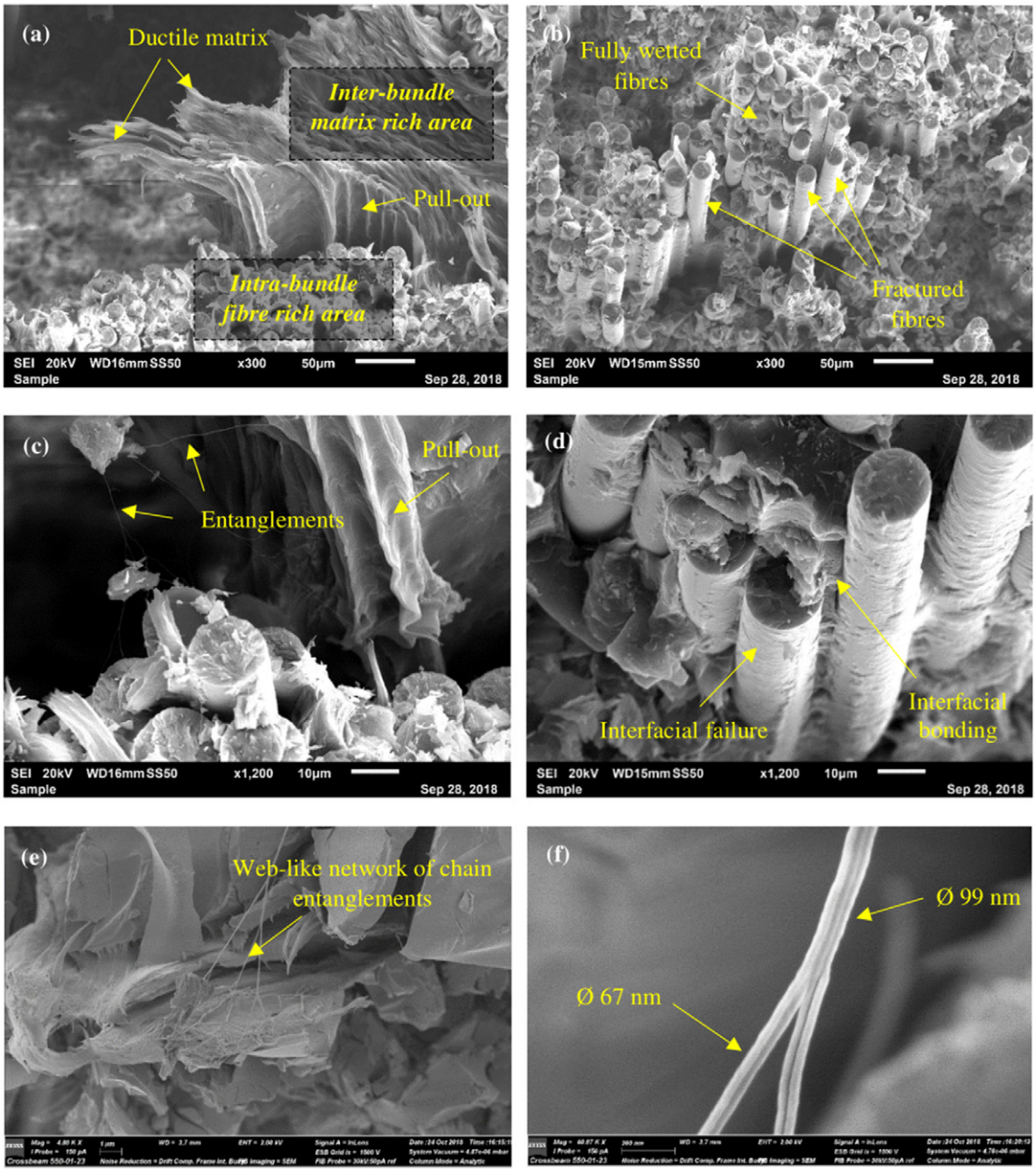

Fig. 14. SEM images of the fractured surface of GF/APA-6 flexural samples.

distribution of inter-bundle voids. Micro CT with higher resolution would render superior image quality allowing for segmentation within bundles, but at the expense of sample size.

3.2. Degree of polymerisation, crystallinity and melt temperatures

The degree of conversion for samples was calculated using Eq. (1) and approximated to be in the 94–95% range. Examples of typical DSC temperature-heat flow results from tested APA-6 and GF/APA-6 samples are presented in Fig. 7. The melt temperatures are similar to that for PA-6 reported in literature [20], though the lower value for the pure APA-6 may indicate that the molecular weight is lower in this study. Due to the composites consisting of ~52% fibres, the apparent enthalpy of fusion results are lower than those for the pure polymer. The fibre content was taken into account in Eq. (2) when calculating the degree of crystallinity and the results are shown in Table 3. This analysis shows that the degree of crystallinity is slightly lower for the polymer than the composite. As the thermal conductivity of the fibres is about 1/5th that of the APA-6, their presence in the composite during processing possibly slows down the transfer of heat during crystallisation, thus resulting in a higher degree of crystallinity. When cooled at a rate of 10 °C/min after melting, the resulting crystallinity is reduced significantly for all three cases. The difference in the degree of crystallinity between the polymer and composite is reduced as a result. This indicates that historical morphological effects, which occurred upon cold crystallisation, and caused a difference between the two due to the presence of fibres; has mostly been eliminated.

3.3. Polymer mechanical properties

The results from the tensile and flexural testing of the pure APA-6 polymer in terms of strength, strain and modulus are summarised in Table 4 and representative stress-strain curves are presented in Fig. 8.

The tensile yield strength in tension was determined where the change in stress with respect to strain ($d\sigma/d\varepsilon$) reached its minimum prior to necking. For each sample set, the stress at the lowest average $d\sigma/d\varepsilon$ over a range of $\pm$50 data points (100 in total) was used to determine the yield point. The maximum strength values are 7–30% higher than those reported in another study for anionically polymerised PA-6 over a wide range of polymerisation temperatures (140 °C - 170 °C) [28] and those produced by hydrolytic polymerisation [20]. Based on the results for density and melt temperature, the molecular weight of the polymer synthesised in the current study is suspected to be slightly higher than that in literature for APA-6 which would partially explain this. The slower reacting catalyst used in the literature [31] would likely have affected the crystallinity, explaining the discrepancy between the reported results and that in the study. It is possible that a higher degree of crystallinity (hence stiffness) and a higher crosshead speed (hence strain rate) during testing would have yielded results more similar to the literature. The strains at maximum strength and break in this work are also higher than those in literature [28], further backing up the above points. In general, a higher percentage amorphous phase per unit volume of a polymer allows for greater extension of its polymer chains, and its load bearing capability is increased by its high molecular weight.

Inspecting the flexural results, it should be noted that the samples were not tested to failure and therefore, results for strain at maximum strength/break could not be determined. However, the flexural stress σ_c at a deflection of 1.5 times the thickness as defined in the test standard [45] was determined to be 86.8 $\pm$ 1.0 MPa. The flexural strength compared to tensile strength is typical for polymers as the upper part of the specimen is in compression and the compressive strength is higher [20]. The results are in the range of those for hydrolytically polymerised PA-6 [20]. Overall, the results relate quite well to one another. The low standard deviation in all cases gives high confidence in the test methodology.

3.4. Composite transverse properties

The transverse properties of the GF/APA-6 composite determined from testing are summarised in Table 5 and representative stress-strain curves are presented in Fig. 9.

Transverse properties in unidirectional composites are dependent on a variety of factors including matrix and fibre properties, interfacial bond strength, the volume and distribution of voids, internal stress-strain distribution and in this case, the stitching [46–48]. The transverse tensile strength for the composite falls well below tensile strength of the pure matrix. This can be explained by stress concentrations due to the fibres which peak midway between two fibres in the matrix. UD composites with fibre volume fractions of ~50% typically have a transverse strength reduction by a factor of ~2 with respect to the matrix tensile strength [46]. This is further reduced by material flaws, and for polymer matrices with non-linear stress-strain relationships (such as that of the pure APA-6 as shown in Fig. 9), the high strain at failure may cause other phenomena to occur which haven't been considered. The fibre bundles which are tightly packed due to the stitching result in local regions with high fibre volume fractions much greater than the composite average (~52%) and inter-bundle regions which are almost exclusively matrix as shown in Fig. 10. A number of these micro-section images were stitched and a region representing one ply shown by the dashed green area in Fig. 10 was analysed. The fibre rich areas were found to have local fibre volume fractions ~65%.

The stitched image in Fig. 10 is an example of a cross-section between two stitches. In the areas where there is stitching every 5 mm along the ply width (~4/5 per ply per sample), the fibres are even more tightly packed. This, combined with a reduced local load bearing area due to voids at these bundle-stitch intersections (as discussed in Section 3.1.3) would likely act as an initiation point for failure (as demonstrated in Fig. 11). After initiation, it is likely that these cracks propagate along the fibre-matrix interface [46]. While the void content is below the critical value (~2%) mentioned in literature [49] at which transverse strength drops off significantly, the bulk distribution of voids occurs along the planes at the mentioned intersections. It is clear from Fig. 10 that the stacking of bundles between plies is not staggered and it would be impractical to purposely do so in reality. Where bundles between plies are aligned, so are the voids along the same plane and as a result, the load bearing area is further reduced, resulting in weak regions in specimens.

In compression, the transverse specimens mostly failed in shear along the gauge length. This failure is typical in unidirectional composites in the transverse direction [46]. In all cases, the shear plane of failure seems to have initiated between bundles on the outer surface and from there on, propagating both through and between bundles showing slight bias towards the latter path.

Flexural testing in the transverse direction resulted in failure occurring from the lower side of the specimen in tension at various locations showing bias towards inter-bundle failure in some cases. The flexural strength falls somewhere between the tensile and compressive strength values as expected.

3.5. Composite longitudinal properties

The longitudinal properties of the GF/APA-6 composite determined from testing are summarised in Table 6 and representative stress-strain data is presented in Fig. 12.

Compared to organo-sheet produced from GF/APA-6 tapes with ~50% fibre volume fraction [50], the tensile longitudinal modulus of the equivalent composite in the current study is lower by about 14% but its strength is higher by about 2%, and the strain-to-failure is higher by about 21%. The difference in modulus may be attributed to the fibre crimp introduced by the polyester stitching, which would also explain the higher strain-to-failure for the current study. At each stitch, the fibres are tightly packed as can be observed in Fig. 1, which causes a

local reduction in fibre straightness. During extension of the samples in the longitudinal direction, straightening of these fibres may occur due to the allowance of transverse strain by the matrix, hence causing larger composite strain and a reduction in modulus. In a study comparing UD carbon fibre composites manufactured from straight fibre tows versus those manufactured from an NCF but using fibres with a similar modulus, it was shown that the modulus for the stitched case was inferior [51,52].

Consistent initial failure occurred across the entire sample set with either splitting through the laminate thickness or from an individual ply (i.e. delamination) such as that in Fig. 13(a). In all cases, the cracks followed clear inter-bundle pathways through the matrix. In some cases, the samples were left in the grips at constant load after initial failure to observe failure progression across the entire specimen without applying any further load. Generally, this occurred within seconds after initial failure in an explosive fashion, though all breakage still occurred around bundles such as that shown in Fig. 13(b). Due to their lower strain-to-failure, it is likely that the failure initiated in a fibre or across a bundle first, followed by propagation along an inter-bundle pathway. Due to the formation of voids at the bundle-stitch intersections, it is understandable that failure propagated along these pathways.

Compressive failure occurred mainly along the net section of specimens due to kinking. A closer observation revealed that the planes of kinking showed bias towards stitched areas where the voids were aligned. Due to the lack of local fibre straightness at stitched locations, the compressive strength is likely reduced; thus, the compression strength is dominated by the shear modulus of the matrix, which is heavily dependent on the degree of crystallisation in the case of the APA-6 matrix [27].

The flexural samples failed at first in compression on the upper surface, which was expected as the compressive strength of the material is lower. Compared to commercial organo-sheet produced from GF/PA-6 tapes with ~50% fibre volume fraction, the mean compressive strength of samples in this work is slightly higher but the mean modulus when normalised is 12.4% less. It is suspected that the lower modulus is due to preliminary straightening of fibre bundles in the lower (tensioned) surface in a similar manner to that described for the tensile 0° samples, so the fibre bundles did not reinforce the specimens to their potential for the initial part of the test.

Scanning electron microscopy images taken of the specimens show the fracture surface in more detail and are described in Section 3.6. A summary of normalised composite mechanical properties are compared to those from commercial organo-sheet in Table 7.

3.6. Scanning electron microscopy

SEM images of the fractured surface of flexural specimens are shown in Fig. 14. The images clearly show the distinct inter-bundle matrix areas and intra-bundle fibre rich areas described previously in Section 3.5. The former demonstrates ductile behaviour of the APA-6 polymer. There are signs of both clean fibre pull-out and remnants of polymer on the surface throughout samples, indicating a satisfactory degree of interfacial adhesion at the fibre-matrix interface. Interestingly, web-like networks were observed in areas across the fracture surfaces, which are believed to be polymer chain entanglements that were stretched during failure. The diameter of the entanglements were measured using *ImageJ* in various locations at higher magnifications and were shown to be in the nanoscale.

4. Conclusions

High quality glass fibre PA-6 composite laminates were successfully manufactured using bespoke TP-RTM equipment, a mould and a pneumatic press. Because the viscosity of the precursor system was significantly lower than those of most epoxies and polyurethanes used in RTM, the pressures and hence equipment cost required, to achieve the same fibre volume fraction and wet-out using TP-RTM were a fraction of those for thermoset RTM [55]. As a result, improved composite properties can be achieved at a much lower cost. The TP-RTM equipment used was relatively inexpensive (~£5000) to build and can be upscaled easily to produce larger parts without increasing the equipment cost significantly. Mechanical, chemical and thermo-morphological testing demonstrated that the material properties compared excellently with commercial organo-sheet produced from GF/PA-6 tapes. Most of the disadvantages associated with the material were a result of defects caused by the stitching during injection. In order to adapt the current setup for high volume manufacturing, the parts would need to be cooled at a faster rate. This study proves that there is vast potential for the use of APA-6 as a composite matrix and provides details which can contribute significantly to broadening their use in applications across various industries where desirable.

CRediT authorship contribution statement

James J. Murray: Conceptualization, Data curation, Formal analysis, Investigation, Methodology, Project administration, Resources, Visualization, Writing - original draft, Writing - review & editing. **Colin Robert:** Data curation, Formal analysis, Investigation, Methodology, Resources, Writing - review & editing. **Klaus Gleich:** Conceptualization, Funding acquisition, Methodology, Project administration, Resources, Supervision, Writing - review & editing. **Edward D. McCarthy:** Conceptualization, Investigation, Methodology, Project administration, Resources, Supervision, Validation, Visualization, Writing - original draft, Writing - review & editing. **Conchúr M.Ó. Brádaigh:** Conceptualization, Funding acquisition, Investigation, Methodology, Project administration, Resources, Supervision, Validation, Visualization, Writing - original draft, Writing - review & editing

Declaration of competing interest

The authors declare that they have no known competing financial interests or personal relationships that could have appeared to influence the work reported in this paper.

Acknowledgements

The authors would like to thank Johns Manville (CO, USA) who have co-funded this work, supplied the fabrics used in the study and provided a lot of expert advice and knowledge. I would like to thank Brüggemann GmbH & Co. KG (Heilbronn, Germany) for providing the caprolactam and all colleagues who supported this work including Mr. Edward Monteith, Dr. Dimitrios Mamalis, Dr. James Maguire and Ms. Evanthia Pappa.

Data availability

The raw/processed data required to reproduce these findings cannot be shared at this time due to technical or time limitations.

References

[1] I.Y. Chang, J.K. Lees, Recent development in thermoplastic composites: a review of matrix systems and processing methods, J. Thermoplast. Compos. Mater. 1 (1988) 277–296, https://doi.org/10.1177/089270578800100305.
[2] L. Ye, V. Klinkmuller, K. Friedrich, Impregnation and consolidation in composites made of GF/PP powder impregnated bundles, J. Thermoplast. Compos. Mater. 5 (1992) 32–48, https://doi.org/10.1177/089270579200500103.
[3] P. McDonnell, K.P. McGarvey, L. Rochford, C.M. Ó Brádaigh, Processing and mechanical properties evaluation of a commingled carbon-fibre/PA-12 composite, Compos. Part A Appl. Sci. Manuf. 32 (2001) 925–932, https://doi.org/10.1016/S1359-835X(00)00155-X.
[4] L.A. Khan, A.H. Mehmood, Cost-effective composites manufacturing processes for automotive applications, Light. Compos. Struct. Transp, Elsevier Ltd 2016, pp. 93–119, https://doi.org/10.1016/B978-1-78242-325-6.00005-0.

[5] European Parliament, Council of the European Union, REGULATION (EU) No 333/2014 OF THE EUROPEAN PARLIAMENT AND OF THE COUNCIL of 11 March 2014 amending Regulation (EC) No 443/2009 to define the modalities for reaching the 2020 target to reduce CO 2 emissions from new passenger cars THE, Off. J. Eur. Union (2014) 15–21.

[6] BMW Group PressClub, The new 2017 BMW i3 (94 Ah): more range paired to high-level dynamic performance, Press Release. (2016).

[7] R. Hitch, CFC Usage and Future Strategy at Jaguar Land Rover, SAMPE UK Irel, 2016.

[8] T. Ishikawa, K. Amaoka, Y. Masubuchi, T. Yamamoto, A. Yamanaka, M. Arai, J. Takahashi, Overview of automotive structural composites technology developments in Japan, Compos. Sci. Technol. 155 (2018) 221–246, https://doi.org/10.1016/j.compscitech.2017.09.015.

[9] C.D. Rudd, A.C. Long, K.N. Kendall, C.G.E. Mangin, C.D. Rudd, A.C. Long, K.N. Kendall, C.G.E. Mangin, 1 – Introduction to liquid composite moulding, Liq. Mould. Technol, 1997, pp. 1–37, https://doi.org/10.1533/9781845695446.1.

[10] W. Obande, D. Mamalis, D. Ray, L. Yang, C.M. Ó Brádaigh, Mechanical and thermomechanical characterisation of vacuum-infused thermoplastic- and thermoset-based composites, Mater. Des. 175 (2019), 107828. https://doi.org/10.1016/j.matdes.2019.107828.

[11] R.E. Murray, D. Swan, D. Snowberg, D. Berry, R. Beach, S. Rooney, Manufacturing a 9-meter thermoplastic composite wind turbine blade, Am. Soc. Compos. 32nd Tech. Conf. (2018) https://doi.org/10.12783/asc2017/15166.

[12] H. Parton, I. Verpoest, In situ polymerization of thermoplastic composites based on cyclic oligomers, Polym. Compos. 26 (2005) 60–65, https://doi.org/10.1002/pc.20074.

[13] J. Baets, A. Godara, J. Devaux, I. Verpoest, Toughening of isothermally polymerized cyclic butylene terephthalate for use in composites, Polym. Degrad. Stab. 95 (2010) 346–352, https://doi.org/10.1016/j.polymdegradstab.2009.11.005.

[14] A. Murtagh, S. Coll, C.M. Ó Brádaigh, Processing of low-viscosity Cbt thermoplastic composites: heat transfer analysis, Composites. (2006) 157–164.

[15] C.M. Ó Brádaigh, A. Doyle, D. Doyle, P.J. Feerick, Electrically-heated ceramic composite tooling for out-of-autoclave manufacturing of large composite structures, SAMPE J. 47 (2011) 6–14. http://apps.webofknowledge.com/full_record.do?product=UA&search_mode=Refine&qid=5&SID=Z1MKW1yFF6LkjG4U9Lm&page=1&doc=1.

[16] T. Ageyeva, I. Sibikin, J. Karger-Kocsis, Polymers and related composites via anionic ring-opening polymerization of lactams: recent developments and future trends, Polymers (Basel) 10 (2018) https://doi.org/10.3390/polym10040357.

[17] J. Šebenda, Anionic Ring-opening Polymerization: Lactams, Compr. Polym. Sci. Suppl, 1989 511–530, https://doi.org/10.1016/B978-0-08-096701-1.00097-5.

[18] K. Udipi, R. Dave, R. Kruse, L. Stebbins, Polyamides from lactams via anionic ring-opening polymerization: 1. Chemistry and some recent findings, Polymer (Guildf) 38 (1997) 927–938, https://doi.org/10.1016/S0032-3861(96)00566-6.

[19] S. Russo, E. Casazza, 4.14 – Ring-opening polymerization of cyclic amides (lactams), Polym. Sci. A Compr. Ref. (2012) 331–396, https://doi.org/10.1016/B978-0-444-53349-4.00109-6.

[20] M. Xenopoulos, A and Clark, ES and A, in: M.I. Kohan (Ed.), Nylon Plastics Handbook, 1, 1995, p. 108, https://doi.org/10.1109/MEI.1996.537196.

[21] A. Luisier, P. Bourban, J. Månson, In situ polymerization of polyamide 12 for thermoplastic composites, Proc. 1999 Int. Conf. Compos. Mater, 1999. http://www.iccm-central.org/Proceedings/ICCM12proceedings/site/papers/pap610.pdf.

[22] L. Zingraff, V. Michaud, P.E. Bourban, J.A.E. Månson, Resin transfer moulding of anionically polymerised polyamide 12, Compos. Part A Appl. Sci. Manuf. 36 (2005) 1675–1686, https://doi.org/10.1016/j.compositesa.2005.03.023.

[23] P. Ó Máirtín, P. McDonnell, M.T. Connor, R. Eder, C.M. Ó Brádaigh, Process investigation of a liquid PA-12/carbon fibre moulding system, Compos. Part A Appl. Sci. Manuf. 32 (2001) 915–923, https://doi.org/10.1016/S1359-835X(01)00005-7.

[24] Hexcel Corporation, HexFlow ® RTM 6 Datasheet, 2018 1–4.

[25] K. van Rijswijk, H.E.N. Bersee, W.F. Jager, S.J. Picken, Optimisation of anionic polyamide-6 for vacuum infusion of thermoplastic composites: choice of activator and initiator, Compos. Part A 37 (2006) 949–956.

[26] K. van Rijswijk, H.E.N. Bersee, Reactive processing of textile fiber-reinforced thermoplastic composites - an overview, Compos. Part A Appl. Sci. Manuf. 38 (2007) 666–681, https://doi.org/10.1016/j.compositesa.2006.05.007.

[27] K. Van Rijswijk, J.J.E. Teuwen, H.E.N. Bersee, A. Beukers, Textile fiber-reinforced anionic polyamide-6 composites. Part I: the vacuum infusion process, Compos. Part A Appl. Sci. Manuf. 40 (2009) 1–10, https://doi.org/10.1016/j.compositesa.2008.03.018.

[28] K. van Rijswijk, H.E.N. Bersee, a Beukers, S.J. Picken, A.A. van Geenen, Optimisation of anionic polyamide-6 for vacuum infusion of thermoplastic composites: influence of polymerisation temperature on matrix properties, Polym. Test. 25 (2006) 392–404, https://doi.org/10.1016/j.polymertesting.2005.11.008.

[29] K. van Rijswijk, A.A. van Geenen, H.E.N. Bersee, Textile fiber-reinforced anionic polyamide-6 composites. Part II: investigation on interfacial bond formation by short beam shear test, Compos. Part A Appl. Sci. Manuf. 40 (2009) 1033–1043, https://doi.org/10.1016/j.compositesa.2009.02.018.

[30] B.J. Kim, S.H. Cha, Y. Bin Park, Ultra-high-speed processing of nanomaterial-reinforced woven carbon fiber/polyamide 6 composites using reactive thermoplastic resin transfer molding, Compos. Part B Eng. 143 (2018) 36–46, https://doi.org/10.1016/j.compositesb.2018.02.002.

[31] P. Rosso, K. Friedrich, A. Wollny, R. Mülhaupt, A novel polyamide 12 polymerization system and its use for a LCM-process to produce CFRP, J. Thermoplast. Compos. Mater. 18 (2005) 77–90, https://doi.org/10.1177/0892705705041987.

[32] L. Zingraff, V. Michaud, P.E. Bourban, J.A.E. Månson, Resin transfer moulding of anionically polymerised polyamide 12, Compos. Part A Appl. Sci. Manuf. 36 (2005) 1675–1686, https://doi.org/10.1016/j.compositesa.2005.03.023.

[33] S. Pillay, U.K. Vaidya, G.M. Janowski, Liquid molding of carbon fabric-reinforced Nylon matrix composite laminates, J. Thermoplast. Compos. Mater. 18 (2005) 509–527, https://doi.org/10.1177/0892705705054412.

[34] N. Müller, P. Seinsche, T-RTM Components from Caprolactam – Performance Characteristics, Processing Aspects and In-line Testing, Employing Active Thermography, SAMPE Eur, Stuttgart, 2017.

[35] S. Schmidhuber, P. Zimmermann, It Couldn't be more hybrid. Thermoplastic-matrix RTM on the roof frame of the Roding roadster, Kunstst. Intl. (2017) 36–38.

[36] M. Bitterlich, Tailored to Reactive Polyamide 6: Thermoplastic Resin Transfer Moulding, 2014 47–51.

[37] A. de la Calle, S. Garcia-Arrieta, C. Elizetxea, In-situ polymerized continuous fiber thermoplastic composite manufactured through liquid molding processes, 16th Eur. Conf. Compos. Mater 2014, pp. 22–26.

[38] O.V. Semperger, A. Suplicz, The effect of the parameters of T-RTM on the properties of polyamide 6 prepared by in situ polymerization, Materials 13 (2020).

[39] K. Chen, M. Jia, H. Sun, P. Xue, Thermoplastic reaction injection pultrusion for continuous glass fiber-reinforced polyamide-6 composites, Materials 12 (2019) https://doi.org/10.3390/ma12030463.

[40] L. Lewerdomski, C. Schütz, Interfacial adhesion optimization using 2-C silane compounds during the T-RTM process, Light. Des. Worldw. (2019) https://doi.org/10.1007/s41777-019-0050-3.

[41] W.V. Steele, R.D. Chirico, S.E. Knipmeyer, A. Nguyen, B.D.M.P. Technologies, P.O. Box, Measurements of vapor pressure, heat capacity, and density along the saturation line for E-caprolactam, pyrazine, 1,2-propanediol, triethylene glycol, phenyl acetylene, and diphenyl acetylene, J. Chem. Eng. 47 (2008) 689–699, https://doi.org/10.1021/je010085z.

[42] K. Ueda, M. Hosoda, T. Matsuda, K. Tai, Synthesis of high molecular weight nylon 6 by anionic polymerization of ε-caprolactam. formation of cyclic oligomers, Polym. J. 30 (1998) 186–191.

[43] H.C.Y. Cartledge, C.A. Baillie, Studies of microstructural and mechanical properties of nylon/glass composite part I the effect of thermal processing on crystallinity, transcrystallinity and crystal phases, J. Mater. Sci. 34 (1999) 5099–5111, https://doi.org/10.1023/A:1004765201803.

[44] ASTM International, ASTM D6641/D6641M-16e1, Standard Test Method for Compressive Properties of Polymer Matrix Composite Materials Using a Combined Loading Compression (CLC) Test Fixture, 2016https://doi.org/10.1520/D6641.

[45] ISO, BSI Standards Publication Plastics — Determination of Flexural Properties, 2013.

[46] F.L. Matthews, R.D. Rawlings, Composite Materials: Science and Engineering, 2nd ed. Springer, New York, 1999https://doi.org/10.1016/S0140-6736(00)67208-2.

[47] B. Li, M. Zhao, X. Wan, The influence of void distribution on transverse mechanical properties of unidirectional composites, 2017 8th Int. Conf. Mech. Aerosp. Eng. ICMAE 2017 2017, pp. 209–214, https://doi.org/10.1109/ICMAE.2017.8038644.

[48] D. Hull, An Introduction to Composite Materials, 1983https://doi.org/10.1016/0378-3804(83)90009-8.

[49] C. Dong, Effects of process-induced voids on the properties of fibre reinforced composites, J. Mater. Sci. Technol. 32 (2016) 597–604, https://doi.org/10.1016/j.jmst.2016.04.011.

[50] SGL Group, Unidirectional Glass Fiber Tape with Thermoplastic Matrix Datasheet, 2017.

[51] J.J. Murray, E.J. Pappa, D. Mamalis, G. Breathnach, A. Doyle, T. Flanagan, S. Di Noi, C.M. Brádaigh, Characterisation of carbon fibre reinforced powder epoxy composites for wind energy blades, Proc. 18th Eur. Conf. Compos. Mater, 2018.

[52] D. Mamalis, J.J. Murray, J. McClements, D. Tsikritsis, V. Koutsos, E.D. McCarthy, C.M. Ó Brádaigh, Novel carbon-fibre powder-epoxy composites: Interface phenomena and interlaminar fracture behaviour, Compos. Part B Eng. 174 (2019) https://doi.org/10.1016/j.compositesb.2019.107012.

[53] Evonik Industrial, VESTAPE Uni-directional Tapes for Structural Lightweight Design Datasheet, (n.d.).

[54] TenCate, TenCate Cetex ® TC910 Datasheet, 2018.

[55] J. Summerscales, Composites Manufacturing for Marine Structures, Elsevier Ltd, 2015https://doi.org/10.1016/B978-1-78242-250-1.00002-8.